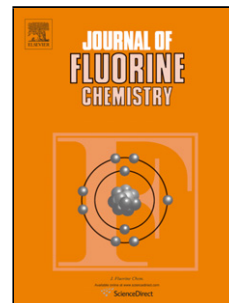


Accepted Manuscript

Title: Multi-color photoluminescence induced by electron-density distribution of fluorinated bistolane derivatives

Authors: Shigeyuki Yamada, Masato Morita, Tsutomu Konno



PII: S0022-1139(17)30375-5
DOI: <http://dx.doi.org/10.1016/j.jfluchem.2017.09.003>
Reference: FLUOR 9044

To appear in: *FLUOR*

Received date: 22-8-2017
Revised date: 4-9-2017
Accepted date: 4-9-2017

Please cite this article as: Shigeyuki Yamada, Masato Morita, Tsutomu Konno, Multi-color photoluminescence induced by electron-density distribution of fluorinated bistolane derivatives, Journal of Fluorine Chemistry <http://dx.doi.org/10.1016/j.jfluchem.2017.09.003>

This is a PDF file of an unedited manuscript that has been accepted for publication. As a service to our customers we are providing this early version of the manuscript. The manuscript will undergo copyediting, typesetting, and review of the resulting proof before it is published in its final form. Please note that during the production process errors may be discovered which could affect the content, and all legal disclaimers that apply to the journal pertain.

Multi-color photoluminescence induced by electron-density distribution of fluorinated bistolane derivatives

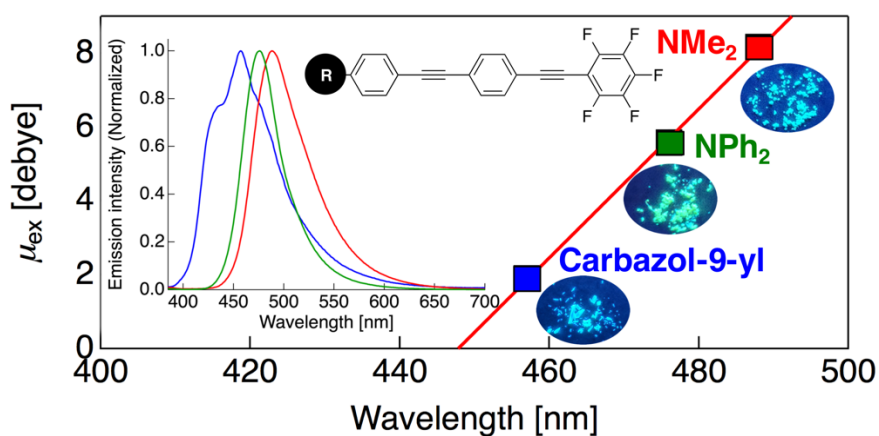
Shigeyuki Yamada,^{a,*} Masato Morita^a and Tsutomu Konno^a

^a Faculty of Molecular Chemistry and Engineering, Kyoto Institute of Technology

Matsugasaki, Sakyo-ku, Kyoto 606-8585, Japan

Tel: +81-75-724-7517; E-mail: syamada@kit.ac.jp

Graphical Abstract



Highlights

- This study clarifies role of molecular design in altering photoluminescence color.
- Fluorinated bistolanes with *N*-type electron-donating substituent were developed.
- They exhibited photoluminescence both in dilute solution and the solid state.
- They exhibited blue to green-color photoluminescence.

Abstract:

The aim of this study was to design and develop new fluorinated light-emitting materials with multi-color photoluminescence that are not limited by their states. For this purpose, fluorinated bistolanes with an amino substituent, such as carbazol-9-yl, diphenylamino, and dimethylamino groups, as an electron-donating moiety were synthesized from readily available *N,N*-disubstituted 4-bromoaniline derivatives through five easy steps. The new fluorinated bistolane derivatives were found to display photoluminescence in dilute solutions as well as in the solid state. The luminescent color varied depending on the type of electron-donating group, and the emission color could be controlled from blue to yellowish-green depending on the electron-density distribution induced by electron-withdrawing pentafluorophenyl and electron-donating amino moieties. Moreover, the bistolanes with a large molecular dipole were found to exhibit solvatochromic photoluminescence. Therefore, multi-color luminescence from blue to yellow could be achieved in a single molecule depending on solvent polarity.

Keyword: Fluorine; Bistolane; Luminescence; Solvatochromism; Electron-density distribution tuning

1. Introduction

Organic light-emitting materials have widespread applications, such as in lighting devices, displays for PC and TV monitors, and medical treatment using fluorescent diagnostics; consequently, they have become one of the most essential materials for human life [1]. Many organic chemists have concentrated on developing innovative luminous molecules, and successfully discovered a number of luminescent molecules.

Such luminescent molecules can be divided into three types depending on the state (Fig. 1). Most fluorescent molecules are generally available only in dilute solutions (Fig. 1A), because their luminescence rapidly diminishes due to a quenching effect known as aggregation-caused quenching (ACQ) in the concentrated solution or solid state [2], and such fluorescent molecules can be applied in molecular-sensing or bio-imaging materials [3]. However, during the past couple of decades, materials that are emissive in the solid state (Fig. 1B) have received considerable attention for practical applications, such as in organic light-emitting displays (OLEDs) and electroluminescent (EL) displays [4]. Several innovative studies that discovered by Tang *et al.* have contributed to the evolutionary discovery of new solid-state luminescent materials and opened avenues for developing the new class of luminous molecules [5,6]. They firstly developed luminous molecules exhibiting intriguing phenomena in that they become non-emissive in dilute solutions but their luminescent intensity is enhanced with the construction of molecular aggregates. Methods of this type of enhancement include aggregation-induced emission enhancement (AIEE) [5] and crystallization-induced emission enhancement (CIEE) [6]. With the rapid expansion of the applicability of luminescent materials, developing efficient luminous molecules not only in solutions but also in the solid state has drawn significant attention, and it has been reported that several bistolane analogues with any substituents at the central aromatic ring display such luminescent properties emitted both in solution and solid states (Fig. 1C) [7,8].

Recently, our research interest has been directed toward the development of novel light-emitting molecules showing such photoluminescence properties classified in Type-C (Fig. 1C), and we also independently succeeded in the development of novel fluorophores, *viz.* fluorine-containing dissymmetric bistolane (**1**, Fig. 1C) that exhibits strong blue photoluminescence ($\Phi_{em} = 0.79$ in solution; $\Phi_{em} = 0.66$ in crystal) under UV irradiation [9]. The photoluminescence in dilute solution as well as in the solid state for **1** is attributable to the electron-density distribution based on the most electronegative fluorine substituents [10,11]. However, such luminous molecules are still not satisfactory because of the

difficulty in achieving a distinct emission behavior [12]. Therefore, development of efficient luminous molecules both in dilute solution and solid states has been recognized as one of the most important issues in the field of luminescent materials.

On the basis of our preliminary investigation [9], in this study, we designed and synthesized new bistolane-based fluorophores with multi-color luminescence that was achieved by controlling the dipole moment caused by the combination of electron-withdrawing pentafluorophenyl and electron-donating amino groups bound to both ends of the molecule. Here was also disclosed the photophysical properties of the fluorophores in detail.

2. Results and discussion

2.1. Molecular design

The essential factors for designing the multi-color luminescent molecules that fulfilled our purpose are as follows:

- (i) Extended π -conjugated system with a linear molecular shape [8], which possesses luminescent property in solution as well as in the solid state. The luminescence in the latter has been reported to be achieved through aggregation-induced planarization [13].
- (ii) Electron-density distribution by electron-rich and -deficient aromatic moieties incorporated in a molecule, in which the molecular orbital and alignment can be controlled through intramolecular charge transfer to alter photoluminescence color [14].

Based on the molecular design and our preliminary understandings, a fluorine-containing bistolane scaffold that possesses extended π -conjugation and constructs planar conformations is suitable as the fundamental backbone. The favorable bias of electron-density distribution caused by the selection of the combination of the electron-donating or -withdrawing substituents can lead to the development of multi-color photoluminescence molecules without depending on either dilute solution or solid state. Accordingly, we selected three candidates **2a–c** with an electron-donating amino group and an electron-withdrawing pentafluorophenyl group, *e.g.* bistolane with carbazol-9-yl **2a**, diphenylamino (Ph_2N) **2b**, and dimethylamino (Me_2N) substituent **2c**.

To evaluate the validity of our molecular design, we initially performed quantum chemical calculations using the density functional theory (DFT) at the B3LYP/cc-pVDZ levels of theory [15,16]. Fig. 2 shows the chemical structures of **1** and **2a–c** and their molecular electrostatic

potential distributions obtained from theoretical calculation.

Fig. 2 shows that the pentafluorophenyl moiety appeared electron-deficient due to the effective decrease in electron-density on the aromatic ring by the electron-withdrawing fluorine substituents, whereas alkoxy- or amino-substituted aromatic ring were found to be electron-rich due to the electron-donating properties. Accordingly, the candidates **2a–c** showed various electron-density distributions owing to the control of electronic structure by altering the electron-donating substituent.

Additionally, in order to obtain information on the molecular orbitals in the excited state, the time-dependent (TD)-DFT calculation was performed at B3LYP/aug-cc-pVDZ levels of theory. Fig. 3 illustrates frontier-molecular orbital distributions for the highest occupied molecular orbital (HOMO) and the lowest unoccupied MO (LUMO) as well as the HOMO–1 or HOMO–2 and LUMO+1 with a relatively large oscillator strength (f). The theoretical parameters obtained by DFT or TD-DFT calculation are listed in Table 1.

Molecular orbitals at the HOMO level in all cases were found to be spread over the electron-rich aromatic ring, whereas the orbital at the LUMO levels was locally distributed at the electron-deficient aromatic moiety (Fig. 3); the HOMO→LUMO transition with a large excited wavelength is likely to be assigned as intramolecular charge transfer (ICT). On the other hand, HOMO–1→LUMO as well as HOMO→LUMO+1 transitions with a small excited wavelength in the allowed electron-transitions seem to originate from π – π^* transitions due to the delocalized molecular orbitals over the entire molecule in the HOMO–1 as well as in LUMO+1. Similarly, HOMO–2→LUMO and HOMO→LUMO transitions in the case of **2a** can also be assigned as π – π^* and ICT transitions, respectively. Owing to the multiple electron transitions in **2a–c**, it is believed that the design of new fluorinated bistolane candidates **2a–c** is potentially appropriate for multi-color luminescent molecules.

2.2. Synthesis and crystal structure

On the basis of the above theoretical investigations, the target fluorine-containing bistolanes **2a–c** were prepared. The synthetic pathway for **2a–c** is shown in Scheme 1.

The target molecule **2a–c** can be synthesized from 4-bromoaniline derivative **3a–c** as a starting molecule through five steps. On treating *N*-(4-bromophenyl)carbazole (**3a**) with (trimethylsilyl)acetylene (1.5 equiv.) in the presence of $\text{Cl}_2\text{Pd}(\text{PPh}_3)_2$ (6 mol%), PPh_3 (10 mol%), and CuI (10 mol%) in Et_3N at 100 °C for 20 h, Pd(0)-catalyzed Sonogashira cross-coupling reaction took place to provide the corresponding coupling product **4a** in 83% yield. The TMS group was easily deprotected by the treatment of **4a** with K_2CO_3 in MeOH to afford the corresponding terminal acetylene **5a** in quantitative yield. Pd(0)-catalyzed Sonogashira cross-coupling reaction of **5a** with 4-(2-trimethylsilyl)ethynyl-1-bromobenzene (1.5 equiv.) readily proceeded to produce the corresponding **6a** in 55% yield. Subsequent cleavage of the TMS group with the same protocol occurred, providing the corresponding **7a** in 65% yield. Finally, Sonogashira cross-coupling reaction of **7a** with bromopentafluorobenzene was allowed to produce the target fluorinated bistolane **2a** in 32% yield. With the same synthetic protocol, other fluorinated bistolane derivatives **2b** and **2c** were successfully synthesized and their molecular structures were fully identified through several spectroscopic analyses, *e.g.* NMR, IR and HRMS, and the purity was verified through elemental analysis to be sufficient for evaluating their optical behavior.

Among the novel fluorinated bistolanes **2a–c**, carbazol-9-yl-substituted **2a** and Ph_2N -substituted **2b** successfully furnished single crystals after purification by column chromatography (eluent: hexane/ CH_2Cl_2 = 5/1), followed by recrystallization from $\text{CH}_2\text{Cl}_2/\text{MeOH}$ (1/1). X-Ray crystallographic analysis of **2a** and **2b** revealed aggregated crystal structures. The obtained crystal structures are shown in Fig. 4.

2a and **2b** were found to crystallize in triclinic $P\bar{1}$ space group and contain two molecules in the crystal lattice. Although three aromatic rings in bistolane derivatives are known to be in a rapid equilibrium between coplanar and twisted conformations *via* free rotation of the alkyne-aryl single bond [13], the crystal structures of **2a** and **2b** were observed

to be coplanar among the three aromatic rings. Both **2a** and **2b** were found to construct molecular aggregates with several π/π interactions between pentafluorophenyl and neighboring benzene rings, indicated as red and blue arrows in Fig. 4b or 4e. In the case of **2a**, the interatomic $\pi\cdots\pi$ distances shown as red and blue arrows were 344 pm and 341 pm, respectively, which are almost equal to the sum of van der Waals radius for two carbons (C: 170 pm) [17]. Additionally, **2a** formed highly ordered structures with intermolecular interactions: CH/ π interaction between the core aromatic π -face and the C–H bond (CH $\cdots\pi$: 318 pm) and hydrogen-bonding interaction between hydrogen and fluorine on the aromatic moiety (H \cdots F: 272 pm). Considering the van der Waals radius of C (170 pm), H (120 pm), F (147 pm) atoms [17], the observed interatomic distances were quite close to the sum of van der Waals radii for two atoms, which means that **2a** in crystal forms molecular aggregate with several weak intermolecular interactions. Similarly, as shown in Figs. 4e and 4f, **2b** formed ordered aggregated structures with multiple π/π and CH/ π intermolecular interactions [18]. Resulting from the crystal structures, it can be concluded that electron-density distribution induced by the electron-donating amino substituent and electronegative fluorine atoms is attributable to the control of molecular alignment in the solid state.

2.3. Photophysical property in dilute solution

Our attention was directed towards investigating the photophysical properties of the designed derivatives. Initially, we measured the absorption behavior of **2** in dilute CH₂Cl₂ solution (10⁻⁵ mol L⁻¹ concentration). Fig. 5a shows the obtained absorption spectra, with the spectrum for **1** also shown for comparison.

Fluorinated bistolane **1** with a methoxy substituent as an electron-donating unit, as previously reported, possessed a single absorption band with an absorption maximum at 322 nm, along with a small shoulder at 350 nm [9]. In contrast, **2a–c** with an amino substituent displayed a distinct spectral shape possessing two or more absorption maxima. Wavelengths at the observed absorption maxima as well as the molar extinction coefficient ($\epsilon/10^3$) are listed in Table 2.

As mentioned earlier, two allowed electron transitions with a relatively large oscillator strength (f) obtained in all molecules were assigned as ICT for HOMO \rightarrow LUMO with a long excited wavelength and $\pi\text{-}\pi^*$ transition for HOMO \rightarrow LUMO+1 (for **1** and **2b–c**) or HOMO-2 \rightarrow LUMO (for **2a**) with a short excited wavelength. Accordingly, the absorption band of **2** in the long-wavelength region can be characterized as the ICT transition, and the other absorption band in the short-wavelength region can be determined as $\pi\text{-}\pi^*$ transitions.

Subsequently, we evaluated the photoluminescence property of bistolanes **2a–c** in dilute solution (10^{-6} mol L $^{-1}$ in CH $_2$ Cl $_2$). Excitation light, with the wavelength of the absorption maximum, was irradiated on the CH $_2$ Cl $_2$ solution of **1** and **2a–c**, and the observed photoluminescence spectra are shown in Fig. 5b. In addition, Fig. 5c shows the Commission Internationale de l'Eclairage (CIE) chromaticity diagram and the photographs of photoluminescence irradiated by UV ($\lambda_{\text{ex}} = 365$ nm). The methoxy-substituted bistolane **1** in dilute solution was reported to show deep blue photoluminescence with an emission maximum at 405 nm [9]. Switching the electron-donating moiety from the methoxy to carbazol-9-yl group, *e.g.* **2a**, a slight shift of emission maxima to the long-wavelength region occurred, resulting in an emission of light-blue photoluminescence. On the other hand, fluorinated bistolane **2b** with Ph $_2$ N-group or **2c** with Me $_2$ N-group in CH $_2$ Cl $_2$ displayed pale-blue photoluminescence with an emission maximum at 495 nm for **2b** and yellowish-green photoluminescence with an emission maximum at 505 nm for **2c**, which were found to dramatically shift to the long-wavelength region by 90–100 nm, compared to **1**. The dramatic change of emission maximum wavelength is attributable to the energy gap between HOMO and LUMO in the excited state. In Fig. 5b, the order of emission bands actually observed was: **1** < **2a** << **2b** < **2c**. Resulting from the HOMO-LUMO energy gaps in the excited states, the theoretical order of the luminescence band followed the order: **1** < **2a** << **2c** < **2b**. As expected, emission bands for **2a–c** appeared in the longer-wavelength region than that for **1**. However, the opposite order was observed between **2b** and **2c** in the actual observation. The opposite order may result from the difference in electron-donating property between Ph $_2$ N and Me $_2$ N groups. Comparing molecular dipole moment (μ_{ex}) in the excited state, the μ_{ex} for **2c** (8.17) was found to be larger than **2b** (5.58). The change of dipole moment can be assumed to cause a wavelength shift of the emission band to the longer-wavelength region. Consequently, the photoluminescence color of the fluorinated bistolane derivatives can be switched depending on

the electron-density distribution, enabled by its significant influence on the energy gap between HOMO and LUMO as well as the molecular dipole moment.

2.4. Solvatochromic photoluminescence property

Much attention has been paid to luminous molecules with a large molecular dipole since they reveal intriguing photoluminescence behavior depending on the solvent polarity, called the solvatochromic photoluminescence property [19,20]. Therefore, we investigated photoluminescence behavior using **2b** (μ_{ex} : 5.58 Debye) as an example for dissolving in a solution with various dielectric constants (ϵ). After preparing the dilute solution (10^{-6} mol L⁻¹) of **2b** with various solvents, such as hexane ($\epsilon = 1.88$), CH₂Cl₂ ($\epsilon = 8.93$), acetone ($\epsilon = 20.6$), and acetonitrile ($\epsilon = 35.9$), photoluminescence properties were observed by irradiation with excitation light at 372 nm, and the spectra observed are shown in Fig. 6a. Fig. 6b shows the CIE diagram obtained from the photoluminescence spectra and photographs of photoluminescence in various solvents under UV irradiation ($\lambda_{\text{ex}} = 365$ nm).

2b in CH₂Cl₂ exhibited pale-blue photoluminescence with a maximum emission wavelength of 495 nm, whereas the **2b** in hexane displayed deep-blue photoluminescence with an emission band at 410 nm with a vibrational structure. In sharp contrast, by switching the solvent from less-polar hexane to more-polar acetone or acetonitrile with a large dielectric constant, the photoluminescence color dramatically changed from deep-blue to yellowish-green in acetone or yellow in acetonitrile. Accordingly, it was clearly demonstrated that the **2b** with a large molecular dipole moment exhibited solvatochromic photoluminescence. The phenomenon of solvatochromic photoluminescence of **2b** can be explained as follows [21]: irradiation of **2b** in the ground state with excitation light promotes the formation of excited species (**2b***), which normally undergoes solvation in the dilute solution state. In the less-polar solvent, the stabilization effect of **2b*** by means of solvation is quite weak, and therefore photoluminescence with high energy occurs, resulting in photoluminescence with an emission band in the short-wavelength region. In the more-polar solvent, **2b*** undergoes strong stabilization by the solvation process through the solvent reorientation, and therefore, the excitation state shifts to lower energy levels, leading to the emission of long-wavelength photoluminescence.

2.5. Photophysical property in the solid state

Furthermore, we evaluated the photoluminescence behavior of the fluorinated bistolane derivatives **2a–c** in the solid state. The observed photoluminescence spectra and CIE color diagram are shown in Fig. 7 and the photophysical data are also listed in Table 3.

As mentioned earlier, methoxy-substituted bistolane **1** displayed strong deep-blue photoluminescence ($\Phi_{em} = 0.66$) [9]. Compounds **2a–c** were found to exhibit photoluminescence even in the solid state; the maximum emission wavelengths were 457 nm for **2a**, 476 nm for **2b**, and 488 nm for **2c** (Fig. 7a, Table 3). As shown in Fig. 7b, the photoluminescence color of **2a–c** were found to switch by changing the substituent at the electron-donating moiety: carbazol-9-yl-substituted **2a** showed blue photoluminescence, Ph₂N-substituted **2b** showed light-blue, and bistolane **2c** with a Me₂N-group exhibited light-green. Our previous paper [9] revealed that the photoluminescence band of the crystal state of the molecule with multiple intermolecular interactions dramatically shifted to the longer-wavelength region compared the photoluminescence band obtained in dilute solution. Comparing photoluminescence behavior of **2a–c** in dilute solution and in the solid state, no large difference could be observed in the photoluminescence wavelength. Photoluminescence in the solid state may be similar to radiation in dilute solution, rather than the radiation from the molecular aggregates, which may be significantly attributable to the molecular orbital of the molecule.

The quantum yield (Φ_{em}) for **1** and **2a–c** was $\Phi_{em} = 0.11–0.66$ (Table 2), which is relatively lower than that of the solution phase. Most luminous molecules are known to rapidly quench in condensed phases (solid state) due to multiple non-radiative processes, such as molecular vibration, rotation, and intermolecular energy transfer. Taking crystal structures for **2a** and **2b** shown in Figs. 4a and 4d into consideration, **2a** and **2b** in the crystal formed coplanar conformation among three aromatic rings, which enhanced intermolecular π/π stacking interaction between two aromatic rings. The π/π interaction may be attributable to the significantly suppressed non-radiative deactivation due to restriction of molecular motion as well as rotation in closely packed structures. Viewing the packing structures carefully, the steric bulkiness of terminal electron-donating substituent, *e.g.* carbazol-9-yl group for **2a** and Ph₂N-group for **2b**, was observed to cause slight sliding along a short molecular axis, which also retarded the non-radiative process by intermolecular energy transfer. These plural effects may promote electron transition *via* the radiative process to induce photoluminescence in the

solid state. On the other hand, the Φ_{em} of **2c** decreased to one-fourth of the Φ_{em} of **2a–b** due to the thermal deactivation caused by the molecular motion due to lack of steric bulk and the high-energy stretching vibration of the sp^3 -hybridized C–H bonds in the NMe₂ group.

2.6. Relationship between photophysical properties and molecular dipole

To investigate the influence of the primary molecular structure on photoluminescence, the correlation between dipole moment in the excited state and photoluminescence maximum wavelength was plotted (Fig. 8).

Plots for **1** were found to be dramatically deviated from the fitting lines, whereas plots for **2a–c** were in alignment with the fitting line in the solid state and slight deviation in solution. The results clearly indicate that no correlation exists between alkoxy-substituted **1** and amino-substituted bistolanes **2a–c**, and a strong correlation was found among **2a–c** with an electron-donating amino group; the photoluminescence color was switched in parallel according to the strength of the electron-donating ability. Overall, the photoluminescence color of fluorinated bistolane derivatives in dilute solution as well as in the solid state can be controlled by the energy gap between HOMO and LUMO of the molecule and dipoles caused by the electron-density distribution.

Conclusions

New fluorinated bistolanes possessing electron-donating amino substituent, such as carbazol-9-yl, Ph₂N-, and Me₂N-group, were designed and synthesized through an easy five-step procedure involving Sonogashira cross-coupling reaction as a key reaction step. After intensive evaluation of their photophysical properties, the developed fluorinated bistolane derivatives were found to exhibit photoluminescence in dilute solution as well as in the solid state. The three kinds of photoluminescence colors—from blue to pale-green—were achieved by the optimal selection of the amino group as the electron-donating substituent of bistolane. In addition, the new bistolane derivatives exhibited a solvatochromic photoluminescence property in that photoluminescence color changed depending on the solvent polarity. From theoretical studies using DFT and TD-DFT, the dramatic color-switching of the photoluminescence can be attributed to the control of energy gap between HOMO and LUMO of the molecule as well as dipoles based on the electron-density distribution induced by strong electronegative fluorine atoms. This study successfully developed novel and high-efficiency luminophores exhibiting blue to green-color photoluminescence. The role

of molecular design in altering photoluminescence color in solution and in the solid state has been disclosed. The findings of this study provide guidelines for molecular design to discover new multi-color luminous materials that are not limited by the state of materials.

4. Experimental

4.1. General

^1H - and ^{13}C -NMR spectra were measured with a Bruker AVANCE III 400 NMR spectrometer (^1H : 400 MHz and ^{13}C : 100 MHz) in chloroform-*d* (CDCl_3) solution and the chemical shifts are reported in parts per million (ppm) using the residual proton in the NMR solvent. ^{19}F -NMR (376 MHz) spectra were measured with a Bruker AVANCE III 400 NMR spectrometer in CDCl_3 solution with CFCl_3 ($\delta_{\text{F}} = 0$ ppm) as an internal standard. Infrared spectra (IR) were determined with the KBr plate method using a JASCO FT/IR-4100 type A spectrometer; all spectra are reported in wavenumber (cm^{-1}). High resolution mass spectra (HRMS) were determined using a JEOL JMS-700MS spectrometer with fast atom bombardment (FAB) methods. Elemental analyses were conducted with a Yanaco CHN CORDER MT-5 instrument. All reactions were carried out using dried glassware with a magnetic stirrer bar. All chemicals were of reagent grade and purified in the usual manner whenever necessary prior to use. Column chromatography was carried out on silica gel (Wakogel® 60N, 38–100 μm) and TLC analysis was performed on silica gel TLC plates (Merck, Silica gel 60 F₂₅₄).

4.2. Typical procedure for the Pd(0)-catalyzed Sonogashira cross-coupling reaction of *N*-4-bromophenyl carbazole (**3a**) with trimethylsilylacetylene

N-4-bromophenyl carbazole (**3a**, 1.6 g, 5.0 mmol), trimethylsilylacetylene (0.76 g, 7.5 mmol), $\text{Cl}_2\text{Pd}(\text{PPh}_3)_2$ (0.10 g, 0.15 mmol), PPh_3 (0.13 g, 0.50 mmol), CuI (0.095 g, 0.50 mmol), and Et_3N (20 mL) were placed in a flask, and the mixture was stirred at 100 °C for 20 h. After stirring, the precipitate formed during the reaction was separated by atmospheric filtration, and the filtrate was poured into a saturated aqueous NH_4Cl solution (20 mL). The crude product was extracted with AcOEt (20 mL) three times and the combined organic layer was washed with brine (once). The organic layer was collected and dried over anhydrous Na_2SO_4 , which was separated by filtration. The filtrate was evaporated *in vacuo* and subjected to silica-gel column chromatography (eluent: hexane/ $\text{CH}_2\text{Cl}_2 = 5/1$) to obtain the coupling product **4a** in 83% yield (1.4 g, 4.3 mmol) as a white solid.

4.2.1. 9-[4-{2-(Trimethylsilyl)ethynyl}phenyl]carbazole (**4a**)

The spectral data were fully in agreement with the reported data [22a]. Yield: 83% (white solid); ¹H NMR (CDCl₃): δ 0.36 (s, 9H), 7.31–7.35 (m, 2H), 7.44–7.45 (m, 4H), 7.55 (d, *J* = 8.8 Hz, 2H), 7.74 (d, *J* = 8.8 Hz, 2H), 8.17 (d, *J* = 7.6 Hz, 2H); ¹³C NMR (CDCl₃): δ –0.03, 95.4, 104.2, 109.7, 120.2, 120.3, 122.1, 123.5, 126.0, 126.7, 133.5, 137.7, 140.5.

4.2.2. 4-{2-(Trimethylsilyl)ethynyl}-*N,N*-diphenylaniline (**4b**)

The spectral data were fully in agreement with the reported data [22b]. Yield: 60% (yellow solid); ¹H NMR (CDCl₃): δ 0.26 (s, 9H), 6.97 (d, *J* = 8.8 Hz, 2H), 7.03–7.14 (m, 6H), 7.24–7.35 (m, 6H); ¹³C NMR (CDCl₃): δ 0.06, 93.0, 105.4, 115.9, 122.1, 123.5, 124.9, 129.3, 132.9, 147.1, 148.0.

4.2.3. 4-{2-(Trimethylsilyl)ethynyl}-*N,N*-dimethylaniline (**4c**)

The spectral data were fully in agreement with the reported data [22c]. Yield: 88% (yellow solid); ¹H NMR (CDCl₃): δ 0.24 (s, 9H), 2.97 (s, 6H), 6.59 (d, *J* = 8.8 Hz, 2H), 7.34 (d, 8.8 Hz, 2H); ¹³C NMR (CDCl₃): δ 0.2, 40.1, 91.1, 106.5, 109.8, 111.5, 133.1, 150.1.

4.3. Typical procedure for the preparation of *N*-(4-ethynylphenyl)carbazole (**5a**)

9-[4-{2-(Trimethylsilyl)ethynyl}phenyl]carbazole (**4a**, 0.68 g, 2.7 mmol), potassium carbonate (0.42 g, 3.0 mmol), and methanol (4.0 mL) were placed in a flask, and the suspension was stirred at room temperature. After stirring for 3 h, the precipitate that was insoluble in the solvent was separated by atmospheric filtration, and the filtrate was poured into saturated aqueous NH₄Cl solution (20 mL). The crude product was extracted with AcOEt (20 mL) three times and the combined organic layer was washed with brine (once). The organic layer was collected and dried over anhydrous Na₂SO₄, which was separated by filtration. The filtrate was evaporated *in vacuo* and subjected to silica-gel column chromatography (eluent: hexane/CH₂Cl₂ = 5/1) to obtain the deprotection product **5a** in 99% yield (0.53 g, 2.0 mmol) as a white solid.

4.3.1. *N*-(4-ethynylphenyl)carbazole (**5a**)

The spectral data were fully in agreement with the reported data [22d]. Yield: 99% (white solid); ¹H NMR (CDCl₃): δ 3.19 (s, 1H), 7.28–7.34 (m, 2H), 7.39–7.46 (m, 4H), 7.56 (d, *J* = 8.4 Hz, 2H), 7.73 (d, *J* = 8.4 Hz, 2H), 8.15 (dt, *J* = 7.6, 1.2 Hz, 2H); ¹³C NMR (CDCl₃): δ 78.1, 82.9, 109.7, 120.2, 120.4, 121.0, 123.5, 126.0, 126.8, 133.6, 138.1, 140.4.

4.3.2. 4-Ethynyl-*N,N*-diphenylaniline (**5b**)

The spectral data were fully in agreement with the reported data [22e]. Yield: 86% (yellow oil); ¹H

NMR (CDCl₃): δ 3.03 (s, 1H), 6.98 (d, J = 8.8 Hz, 2H), 7.07 (tt, J = 6.0, 1.2 Hz, 2H), 7.09–7.14 (m, 4H), 7.24–7.31 (m, 4H), 7.34 (d, J = 8.8 Hz, 2H); ¹³C NMR (CDCl₃): δ 76.3, 83.8, 114.7, 122.0, 123.5, 124.9, 129.3, 133.0, 147.0, 148.2.

4.3.3. 4-Ethynyl-*N,N*-dimethylaniline (**5c**)

The spectral data were fully in agreement with the reported data [22c]. Yield: 99% (brown solid); ¹H NMR (CDCl₃): δ 2.98 (s, 7H, N(CH₃)₂ and C≡CH), 6.62 (d, J = 8.8 Hz, 2H), 7.37 (d, J = 8.8 Hz, 2H); ¹³C NMR (CDCl₃): δ 40.1, 74.7, 84.8, 108.6, 111.6, 133.1, 150.3.

4.4. Typical procedure for the Pd(0)-catalyzed Sonogashira cross-coupling reaction of **5a** with 4-{2-(trimethylsilyl)ethynyl}-1-bromobenzene

N-(4-ethynyl)phenylcarbazole (**5a**, 0.53 g, 2.0 mmol), 4-{2-(trimethylsilyl)ethynyl}-1-bromobenzene (0.76 g, 3.0 mmol), Cl₂Pd(PPh₃)₂ (0.084 g, 0.12 mmol), PPh₃ (0.052 g, 0.20 mmol), CuI (0.038 g, 0.20 mmol), and Et₃N (20 mL) were placed in a flask, and the mixture was stirred at 100 °C for 15 h. After stirring, the resulting precipitate was separated by atmospheric filtration, and the filtrate was poured into saturated aqueous NH₄Cl solution (20 mL). The crude product was extracted with AcOEt (20 mL) three times and the combined organic layer was washed with brine (once). The organic layer was collected and dried over anhydrous Na₂SO₄, which was separated by filtration. The filtrate was evaporated *in vacuo* and subjected to silica-gel column chromatography (eluent: hexane/CH₂Cl₂ = 5/1) to obtain the coupling product **6a** in 55% yield (0.48 g, 1.1 mmol) as a white solid.

4.4.1. *N*-[4-{4-(2-(Trimethylsilyl)ethynyl)phenyl}ethynyl]carbazole (**6a**)

The spectral data were fully in agreement with the reported data [21f]. Yield: 55% (white solid); ¹H NMR (CDCl₃): δ 0.27 (s, 9H), 7.28–7.33 (m, 2H), 7.40–7.45 (m, 2H), 7.48 (d, J = 8.4 Hz, 1H), 7.51 (d, J = 8.8 Hz, 1H), 7.58 (d, J = 8.4 Hz, 2H), 7.75 (d, J = 8.4 Hz, 2H), 8.15 (d, J = 8.0 Hz, 2H); ¹³C NMR (CDCl₃): δ -0.07, 89.9, 90.6, 96.5, 104.6, 109.7, 120.2, 120.4, 121.9, 123.1, 123.2, 123.6, 126.0, 126.8, 131.4, 131.9, 133.1, 137.8, 140.5.

4.4.2. 4-[4-{2-(Trimethylsilyl)ethynyl}phenyl]ethynyl-*N,N*-diphenylaniline (**6b**)

The spectral data were fully in agreement with the reported data [22f]. Yield: 49% (yellow solid); ¹H NMR (CDCl₃): δ 0.26 (s, 9H), 7.00 (d, J = 8.8 Hz, 2H), 7.07 (tt, J = 7.2, 1.2 Hz, 2H), 7.09–7.14 (m, 4H), 7.25–7.35 (m, 4H), 7.36 (d, J = 8.8 Hz, 2H), 7.43 (s, 4H); ¹³C NMR (CDCl₃): δ -0.07, 88.3, 91.7, 96.0, 104.8, 115.6, 122.0, 122.4, 123.6, 123.7, 125.0, 129.4, 131.2, 131.8, 132.5, 147.0,

148.0.

4.4.3. 4-[4-{2-(Trimethylsilyl)ethynyl}phenyl]ethynyl-*N,N*-dimethylaniline (**6c**)

The spectral data were fully in agreement with the reported data [22g]. Yield: 66% (yellow solid); ¹H NMR (CDCl₃): δ 0.25 (s, 9H), 3.00 (s, 6H), 6.66 (d, *J* = 9.2 Hz, 2H), 7.40 (d, *J* = 9.2 Hz, 2H), 7.41 (s, 4H); ¹³C NMR (CDCl₃): δ -0.06, 40.2, 87.2, 92.8, 95.7, 104.9, 109.6, 111.8, 121.9, 124.3, 131.0, 131.8, 132.8, 150.2.

4.5. Typical procedure for the preparation of *N*-[4-{4-(2-ethynyl)phenyl}ethynyl]phenylcarbazole (**7a**)

N-[4-{4-(2-(Trimethylsilyl)ethynyl)phenyl}ethynyl]carbazole (**6a**, 0.48 g, 1.1 mmol), potassium carbonate (0.23 g, 1.7 mmol), and methanol (4.0 mL) were placed in a flask, and the suspension was stirred at room temperature for 3 h. The resulting precipitate was insoluble in the solvent. After consuming the initial **4a**, the precipitate was separated by atmospheric filtration, and the filtrate was poured into saturated aqueous NH₄Cl solution (20 mL). The crude product was extracted with AcOEt (20 mL) three times and the combined organic layer was washed with brine (once). The organic layer was collected and dried over anhydrous Na₂SO₄, which was separated by filtration. The filtrate was evaporated *in vacuo* and subjected to silica-gel column chromatography (eluent: hexane/CH₂Cl₂ = 5/1) to obtain the deprotection product **7a** in 65% yield (0.26 g, 0.71 mmol) as a white solid.

4.5.1. *N*-[4-{4-(2-ethynyl)phenyl}ethynyl]phenylcarbazole (**7a**)

Yield: 65% (white solid); M.p.: 170–171 °C; ¹H NMR (CDCl₃): δ 3.20 (s, 1H), 7.31 (ddd, *J* = 7.6, 6.4, 2.0 Hz, 2H), 7.40–7.47 (m, 4H), 7.50 (d, *J* = 8.4 Hz, 2H), 7.53 (d, *J* = 8.4 Hz, 2H), 7.59 (d, *J* = 8.8 Hz, 2H), 7.76 (d, *J* = 8.8 Hz, 2H), 8.15 (d, *J* = 8.0 Hz, 2H); ¹³C NMR (CDCl₃): δ 79.0, 83.2, 89.7, 90.6, 109.7, 120.2, 120.4, 121.8, 122.1, 123.5, 123.6, 126.0, 126.8, 131.5, 132.1, 133.1, 137.8, 140.5; IR (KBr) ν 3285, 1450, 1334, 1225, 836 cm⁻¹; HRMS (FAB) Calcd for (M⁺) C₂₈H₁₇N: 367.1361, found: 367.1367.

4.5.2. 4-[4-(2-Ethynylphenyl)ethynyl]phenyl-*N,N*-diphenylaniline (**7b**)

The spectral data were fully in agreement with the reported data [22h]. Yield: 85% (yellow solid); ¹H NMR (CDCl₃): δ 3.17 (s, 1H), 7.01 (d, *J* = 8.8 Hz, 2H), 7.07 (tt, *J* = 7.2, 1.2 Hz, 2H), 7.10–7.15 (m, 4H), 7.25–7.32 (m, 2H), 7.37 (d, *J* = 8.8 Hz, 2H), 7.46 (s, 4H); ¹³C NMR (CDCl₃): δ 78.7, 83.4, 88.1, 91.8, 115.5, 121.4, 122.1, 123.6, 124.1, 125.0, 129.4, 131.3, 132.0, 132.5, 147.1, 148.1.

4.5.3. 4-[4-(2-Ethynylphenyl)ethynyl]phenyl-*N,N*-dimethylaniline (**7c**)

The spectral data were fully in agreement with the reported data [22g]. Yield: 66% (yellow solid); ¹H NMR (CDCl₃): δ 3.00 (s, 6H), 3.15 (s, 1H), 6.66 (d, *J* = 8.8 Hz, 2H), 7.40 (d, *J* = 8.8 Hz, 2H), 7.44 (s, 4H); ¹³C NMR (CDCl₃): δ 40.2, 78.4, 85.5, 87.0, 92.9, 109.5, 111.8, 120.8, 124.8, 131.0, 132.0, 132.8, 150.2.

4.6. Typical procedure for the synthesis of

4-[2-{4-(2-(2,3,4,5,6-pentafluorophenyl)ethynyl)phenyl}ethynyl]phenylcarbazole (**2a**)

Cl₂Pd(PPh₃)₂ (0.029 g, 0.042 mmol), PPh₃ (0.018 g, 0.070 mmol), CuI (13 mg, 0.070 mmol), terminal acetylene **7a** (0.26 g, 0.70 mmol), bromopentafluorobenzene (0.25 g, 1.0 mmol) and triethylamine (20 mL) were placed in a 50 mL two-necked round-bottomed flask. The flask was equipped with a stirrer bar, a reflux condenser, and an inlet tube for argon. The mixture was subsequently stirred at 100 °C for 15 h. After stirring, the resultant product was cooled to room temperature, followed by evaporation to remove the solvent. The crude product was extracted with AcOEt (20 mL) and washed with saturated aqueous NH₄Cl solution (20 mL) three times and brine (once). The combined organic layers were dried over anhydrous Na₂SO₄, filtered, and concentrated *in vacuo*. The filtrate was then subjected to silica-gel column chromatography (eluent: hexane/CH₂Cl₂ = 5/1), followed by recrystallization from a mixed solvent (CH₂Cl₂/methanol = 1/1), to obtain the corresponding bistolane **2a** in 32% yield (0.12 g, 0.23 mmol) as a yellow solid.

4.6.1. 4-[2-{4-(2-(2,3,4,5,6-Pentafluorophenyl)ethynyl)phenyl}ethynyl]phenylcarbazole (**2a**)

Yield: 32% (yellow solid); M.p.: 221–222 °C; ¹H NMR (CDCl₃): δ 7.29–7.33 (m, 2H), 7.41–7.47 (m, 4H), 7.59–7.61 (m, 6H), 7.76–7.79 (m, 2H); ¹³C NMR (CDCl₃): δ 75.0–75.1 (m, 1C), 89.8, 91.4, 100.2 (td, *J* = 18.5, 4.2 Hz), 101.1–101.2 (m), 109.9, 120.4, 120.5, 121.6, 121.8, 123.8, 124.6, 126.2, 127.0, 131.9, 132.0, 133.3, 136.4–139.3 (m), 138.1, 140.4–143.1 (m), 140.6, 145.8–148.6 (m); ¹⁹F NMR (CDCl₃): δ –136.33 (dd, *J* = 20.7, 3.5 Hz, 2F), –152.71 (t, *J* = 20.7 Hz, 1F); –162.11 (td, *J* = 20.7, 6.7 Hz, 2F); IR (KBr): ν 3094, 2214, 1923, 1522, 1449, 1229, 989 cm⁻¹; HRMS (FAB+) *m/z* [M⁺] Calcd for C₃₄H₁₆F₅N: 533.1203; found: 533.1248; Anal. Calcd for C₃₄H₁₆F₅N: C, 76.55; H, 3.02; N, 2.63. found: C, 76.55; H, 3.25; N, 2.80.

4.6.2.

N-4-[2-{4-([2-(2,3,4,5,6-Pentafluorophenyl)ethynyl]phenyl)ethynyl]phenyl-*N,N*-diphenylamine (**2b**)

Yield: 61% (yellow solid); M.p.: 184–185 °C; ¹H NMR (CDCl₃): δ 6.99–7.03 (m, 2H), 7.06–7.14

(m, 6H), 7.26–7.31 (m, 4H), 7.36–7.39 (m, 2H), 7.50–7.55 (m, 4H); ^{13}C NMR (CDCl_3): δ 74.6 (d, $J = 3.7$ Hz), 88.1, 92.6, 100.2 (td, $J = 17.6, 4.3$ Hz), 101.3 (d, $J = 3.2$ Hz), 115.3, 120.6, 122.0, 123.7, 125.1, 129.4, 131.4, 131.8, 132.6, 136.2–139.1 (m, 1C), 140.0–142.9 (m, 1C), 145.7–148.4 (m, 1C), 147.0, 148.3, one carbon in pentafluorophenyl was overlapped with other carbons; ^{19}F NMR (CDCl_3): δ -136.99 (dd, $J = 20.7, 6.9$ Hz, 2F), -153.54 (t, $J = 20.7$ Hz, 1F), -162.79 (td, $J = 20.7, 6.9$ Hz, 2F); IR (KBr): ν 3063, 3034, 2202, 1589, 1524, 1496, 1272, 988, 835 cm^{-1} ; HRMS (FAB+) m/z [M^+] Calcd for $\text{C}_{34}\text{H}_{18}\text{F}_5\text{N}$: 535.1359; found: 535.1354; Anal. Calcd for $\text{C}_{34}\text{H}_{18}\text{F}_5\text{N}$: C, 76.26; H, 3.39; N, 2.62. found: C, 76.47; H, 3.43; N, 2.61.

4.6.3. *N,N*-Dimethyl-4-[2-{4-(2-(2,3,4,5,6-pentafluorophen-yl)ethynyl)phenyl}ethynyl]aniline (**2c**)

Yield: 32% (yellow solid); M.p.: 210–212 °C; ^1H NMR (CDCl_3): δ 3.01 (s, 6H), 6.65–6.68 (m, 2H), 7.40–7.43 (m, 2H), 7.48–7.54 (m, 4H); ^{13}C NMR (CDCl_3): δ 40.3, 74.5 (d, $J = 4.1$ Hz), 87.2, 93.9, 100.5 (d, $J = 4.6$ Hz), 101.7 (d, $J = 3.7$ Hz), 109.6, 111.9, 120.3, 125.9, 131.4, 131.9, 133.0, 136.4–139.3 (m), 140.2–143.0 (m), 145.8–148.6 (m), 150.5; ^{19}F NMR (CDCl_3): δ -136.51 (dd, $J = 21.4, 14.1$ Hz, 2F), -153.19 (t, $J = 21.4$ Hz, 1F), -162.31 (td, $J = 21.4, 6.7$ Hz, 2F); IR (KBr): ν 3091, 3032, 2960, 2920, 2849, 2203, 1611, 1597, 1496, 1366, 1138, 983, 835 cm^{-1} ; HRMS (FAB+) m/z [M^+] Calcd for $\text{C}_{24}\text{H}_{14}\text{F}_5\text{N}$: 411.1046; found: 411.1043; Anal. Calcd for $\text{C}_{24}\text{H}_{14}\text{F}_5\text{N}$: C, 70.07; H, 3.43; N, 3.40. found: C, 69.68; H, 3.63; N, 3.30.

4.7. X-Ray crystallographic analysis

Yellow-colored crystals of fluorinated bistolanes with a carbazol-9-yl unit (**2a**) and a diphenylamino group (**2b**) both with approximate dimensions of $0.15 \times 0.10 \times 0.10$ mm were mounted on a glass fiber. The omega scanning technique was used to collect the reflection data using a Bruker D8 goniometer with monochromatized Mo $K\alpha$ radiation ($\lambda = 0.71075$ Å). The initial structure of the unit cell was determined by a direct method using APEX2. The structural model was refined by a full-matrix least-squares method using SHELXL-2014/6 [23]. All calculations were performed using the SHELXL program. The crystal data is summarized as follows:

Compound **2a**: $\text{C}_{34}\text{H}_{16}\text{F}_5\text{N}$, $M = 533.48$, triclinic, $a = 9.5231(10)$, $b = 10.6983(11)$, $c = 14.0307(14)$ Å, $\alpha = 95.981(3)$, $\beta = 109.238(3)$, $\gamma = 103.197(3)^\circ$, $V = 1288.7(2)$ Å³, $T = 296$ K, space group $P-1$, $Z = 2$, 7524 reflections measured, 4330 uniques ($R_{\text{int}} = 0.0973$), which were used in all calculations. The final R_1 and wR_2 were 0.0579 and 0.1842, respectively, ($I > 2\sigma(I)$).

Compound **2b**: $\text{C}_{34}\text{H}_{18}\text{F}_5\text{N}$, $M = 535.49$, triclinic, $a = 5.9072(5)$, $b = 11.4122(10)$, $c = 20.3304(18)$ Å, $\alpha = 78.195(3)$, $\beta = 85.853(3)$, $\gamma = 82.326(2)^\circ$, $V = 1328.1(2)$ Å³, $T = 296$ K, space group $P-1$, $Z = 2$, 4554 reflections measured, 2836 uniques ($R_{\text{int}} = 0.1009$), which were used in all calculations.

The final R_1 and wR_2 were 0.0636 and 0.1821, respectively, ($I > 2\sigma(I)$).

Indexed data have been deposited in the Cambridge Crystallographic Data Centre (CCDC) database (CCDC 1565483 for **2a** and 1565484 for **2b**). Copy of the data can be obtained, free of charge, on application to CCDC, 12 Union Road, Cambridge CB2 1EZ, UK, (fax: +44 1223 336033 or e-mail: deposit@ccdc.cam.ac.uk).

4.8. Computation

All computations were performed using the Gaussian 09 program package (Rev. C.01) [15] and density functional theory (DFT) method. We used the standard basis set, cc-pVDZ levels of theory for geometry optimizations.[16] Stationary points were characterized by frequency calculations to confirm a correct number of imaginary frequencies. Minimum energy structures have no imaginary frequency. The vertical excitation energies and oscillator strengths were estimated for the 6 lowest $S_0 \rightarrow S_1$ transitions using TD-DFT with the same hybrid functional and basis set.

4.9. Photophysical properties

UV-vis absorption spectra were recorded using a JASCO V-630 absorption spectrometer. Steady-state photoluminescence spectra were obtained using a JASCO FP-8500 fluorescence spectrometer. Photoluminescence quantum yields were estimated using a calibrated integrating sphere system (JASCO).

Acknowledgements

The present work was partially supported by the Hitachi-Metals•Materials Science Foundation. The authors are sincerely grateful to Prof. Osamu Tsutsumi at Ritsumeikan University for his kind assistance in X-ray crystallographic analyses. We also acknowledge Profs. Kensuke Naka and Hiroaki Imoto at Kyoto Institute of Technology for their helpful support in photoluminescence measurements.

References

- [1] (a) For selected review, see: J. Zhou, W. Feng, Y. Sun, F. Li, Upconversion luminescent materials: advances and applications, *Chem. Rev.* 115 (2015) 395–465.
(b) Y. Yang, Q. Zhao, W. Feng, F. Li, Luminescent chemodosimeters for bioimaging, *Chem. Rev.* 113 (2013) 197–270.
(c) J.–C.G. Bünzli, Lanthanide luminescence for biomedical analyses and imaging, *Chem. Rev.* 110 (2010) 2729–2755.
- [2] (a) M. Shimizu, T. Hiyama, Organic fluorophores exhibiting highly efficient photoluminescence in the solid state, *Chem. Asian J.* 5 (2010) 1516–1531.
(b) A.C. Grimsdale, K.L. Chan, R.E. Martin, P.G. Jokisz, A.B. Holmes, Synthesis of light-emitting conjugated polymers for applications in electroluminescent devices, *Chem. Rev.* 109 (2009) 897–1091.
(c) J.Z. Liu, J.W.Y. Lam, B.Z. Tang, Acetylenic Polymers: Syntheses, Structures, and Functions, *Chem. Rev.* 109 (2009) 5799–5867.
- [3] For recent reviews, see: (a) V. Gujrati, A. Mishra, V. Ntziachristos, Molecular imaging probes for multi-spectral optoacoustic tomography, *Chem. Commun.* 53 (2017) 4653–4672.
(b) E. Hemmer, P. Acosta-Mora, J. Méndez-Ramos, S. Fischer, Optical nanoprobe for biomedical applications: shining a light on upconverting and near-infrared emitting nanoparticles for imaging, thermal sensing, and photodynamic therapy, *J. Mater. Chem. B* 5 (2017) 4365–4392.
(c) J.–T. Hou, W.X. Ren, K. Li, J. Seo, A. Sharma, X.–Q. Yu, J.S. Kim, Fluorescent bioimaging of pH: from design to applications, *Chem. Soc. Rev.* 46 (2017) 2076–2090.
- [4] (a) For selected review, see: (a) O. Ostroverkhova, Organic Optoelectronic Materials: Mechanisms and Applications *Chem. Rev.* 116 (2016) 13279–13412.
(b) *Physics of Organic Semiconductors*, W. Brütting and C. Adachi (Eds.), Wiley-VCH, Weinheim, Germany, 2012.
(c) K. Zhou, H. Dong, H.–L. Zhang, W. Hu, High performance n-type and ambipolar small organic semiconductors for organic thin film transistors, *Phys. Chem. Chem. Phys.* 16 (2014) 22448–22457.
- [5] (a) J. Mei, N.L.C. Leung, R.T.K. Kwok, J.W.Y. Lam, B.Z. Tang, Aggregation-Induced Emission: Together We Shine, United We Soar!, *Chem. Rev.* 115 (2015) 11718–11940.
(b) *Aggregation-Induced Emission: Fundamentals*, A. Qin and B.Z. Tang (Eds.), John Wiley & Sons, Ltd, Chichester, 2013.
(c) Y. Hong, J.W.Y. Lam, B.Z. Tang, Aggregation-induced emission, *Chem. Soc. Rev.* 40

(2011) 5361–5388.

(d) J. Luo, Z. Xie, J.W.Y. Lam, L. Cheng, H. Chen, C. Qiu, H.S. Kwok, X. Zhan, Y. Liu, D. Zhu, B.Z. Tang, Aggregation-induced emission of 1-methyl-1,2,3,4,5-pentaphenylsilole, *Chem. Commun.* (2001) 1740–1741.

[6] (a) W.Z. Yuan, Y. Zhang, B.Z. Tang, in *Aggregation-Induced Emission: Applications*, A. Qin and B.Z. Tang (Eds.), John Wiley & Sons, Ltd. Chichester, 2013, ch. 2, pp. 43–60.

(b) W.Z. Yuan, X.Y. Shen, H. Zhao, J.W.Y. Lam, L. Tang, P. Lu, C. Wang, Y. Liu, Z. Wang, Q. Zheng, J.Z. Sun, Y. Ma, B.Z. Tang, Crystallization-induced phosphorescence of pure organic luminogens at room temperature, *J. Phys. Chem. C*, 114 (2010) 6090–6099.

(c) Y. Gong, G. Chen, Q. Peng, W.Z. Yuan, Y. Xie, S. Li, Y. Zhang, B.Z. Tang, Achieving persistent room temperature phosphorescence and remarkable mechanochromism from pure organic luminogens, *Adv. Mater.* 27 (2015) 6195–6201.

(d) Y. Dong, J.W.Y. Lam, A. Qin, Z. Li, J. Sun, H.H.–Y. Sun, I.D. Williams, B.Z. Tang, Switching the light emission of (4-biphenyl)phenyldibenzofulvene by morphological modulation: crystallization-induced emission enhancement, *Chem. Commun.* (2007) 40–42.

[7] (a) H. Li, D.R. Powell, R.K. Hayashi, R. West, Poly((2,5-dialkoxy-*p*-phenylene)ethynylene-*p*-phenyleneethynylene)s and Their Model Compounds, *Macromolecules* 31 (1998) 52–58.

(b) C.–H. Zhao, A. Wakamiya, Y. Inukai, S. Yamaguchi, Highly Emissive Organic Solids Containing 2,5-Diboryl-1,4-phenylene Unit, *J. Am. Chem. Soc.* 128 (2006) 15934–15935.

[8] For related reports on the luminous property of bistolane derivatives, see: (a) A. Beeby, K. Frindlay, P.J. Low, T.B. Marder, A re-evaluation of the photophysical properties of 1,4-bis(phenylethynyl)benzene: a model for poly(phenyleneethynylene), *J. Am. Chem. Soc.* 124 (2002) 8280–8284.

(b) C.–H. Zhao, A. Wakamiya, Y. Inukai, S. Yamaguchi, Highly emissive organic solids containing 2,5-diboryl-1,4-phenylene unit, *J. Am. Chem. Soc.* 128 (2006) 15934–15935.

(c) G. Mao, A. Orita, L. Fenenko, M. Yahiro, C. Adachi, J. Otera, Blue emitting fluorophores of phenyleneethynylenes substituted by diphenylethenyl terminal groups for organic light-emitting diodes, *Mater. Chem. Phys.* 115 (2009) 378–384.

(d) R. Thomas, S. Verghese, G.U. Kulkarni, The influence of crystal packing on the solid state fluorescence behavior of alkyloxy substituted phenyleneethynylenes, *J. Mater. Chem.* 19 (2009) 4401–4406.

(e) L. Zhao, I.F. Perepichka, F. Türksoy, A.S. Batsanov, A. Beeby, K.S. Findlay, M.R. Bryce, 2,5-Di(aryleneethynyl)pyrazine derivatives: synthesis, structural and optoelectronic properties,

and light-emitting device, *New J. Chem.* 28 (2004) 912–918.

(f) A. Beeby, K.S. Findlay, P.J. Low, T.B. Marder, P. Matousek, A.W. Parker, S.R. Rutter, M. Towrie, Studies of the S1 state in a prototypical molecular wire using picosecond time-resolved spectroscopies, *Chem. Commun.* (2003) 2406–2407.

(g) F. Maya, S.H. Chanteau, L. Cheng, M.P. Stewart, J.M. Tour, Synthesis of Fluorinated Oligomers toward Physical Vapor Deposition Molecular Electronics Candidates, *Chem. Mater.* 17 (2005) 1331–1345.

[9] S. Yamada, K. Miyano, T. Konno, T. Agou, T. Kubota, T. Hosokai, Fluorine-containing bistolanes as light-emitting liquid crystalline molecules, *Org. Biomol. Chem.* 15 (2017) 5949–5958.

[10] For selected books described general information of fluorine chemistry, see: T. Hiyama, *Organofluorine Compounds, Chemistry and Applications*, Springer-Verlag, Berlin, 2000.

[11] For related reports on fluorine-containing functional molecules, see: (a) S. Yamada, S. Yamaguchi, O. Tsutsumi, Electron-density distribution tuning for enhanced thermal stability of luminescent gold complexes, *J. Mater. Chem. C* 5 (2017) 7977–7984.

(b) S. Yamada, K. Kinoshita, S. Iwama, T. Yamazaki, T. Kubota, T. Yajima, K. Yamamoto, S. Tahara, Synthesis of perfluoroalkylated pentacenes and evaluation of their fundamental physical properties, *Org. Biomol. Chem.* 15 (2017) 2522–2535.

(c) S. Yamada, S. Hashishita, T. Asai, T. Ishihara, T. Konno, Design, synthesis and evaluation of new fluorinated liquid crystals bearing a CF₂CF₂ fragment with negative dielectric anisotropy, *Org. Biomol. Chem.* 15 (2017) 1495–1509.

(d) S. Yamada, S. Hashishita, H. Konishi, Y. Nishi, T. Kubota, T. Asai, T. Ishihara, T. Konno, New entry for fluorinated carbocycles: Unprecedented 3,6-disubstituted 1,1,2,2-tetrafluorocyclohexane derivatives, *J. Fluorine Chem.* 200 (2017) 47–58.

[12] (a) H. Noguchi, T. Hirose, S. Yokoyama, K. Matsuda, Fluorescence behavior of 2,6,10-trisubstituted 4,8,12-triazatriangulene cations in solution and in the solid state, *CrystEngComm* 18 (2016) 7377–7383.

(b) P. Vashishtha, J. E. Halpert, Field-driven ion migration and color instability in red-emitting mixed halide perovskite nanocrystal light-emitting diodes, *Chem. Mater.* 29 (2017) 5965–5973.

[13] (a) M. Levitus, K. Schmieder, H. Ricks, K.D. Shimizu, U.H.F. Bunz, M.A. Garcia-Garibay, Steps to demarcate the effects of chromophore aggregation and planarization in poly(phenyleneethynylene)s. 1. Rotationally interrupted conjugation in the excited states of 1,4-bis(phenylethynyl)benzene, *J. Am. Chem. Soc.* 123 (2001) 4259–4265.

(b) H. Li, D.R. Powell, T.K. Firman, R. West, Structures and photophysical properties of

model compounds for aryethylene disilylene polymers, *Macromolecules* 31 (1998) 1093–1098.

- [14] For selected reviews, see: (a) X. Liu, J. M. Cole, Z. Xu, Substantial intramolecular charge transfer induces long emission wavelengths and mega stokes shifts in 6-aminocoumarins, *J. Phys. Chem. C* 121 (2017) 13274–13279.
- (b) Z.R. Grabowski, K. Rotkiewicz, W. Rettig, Structural Changes Accompanying Intramolecular Electron Transfer: Focus on Twisted Intramolecular Charge-Transfer States and Structures, *Chem. Rev.* 103 (2003) 3899–4032.
- (c) M.R. Bryce, Tetrathiafulvalenes as π -electron donors for intramolecular charge-transfer materials, *Adv. Mater.* 11(1999) 11–23.
- [15] M.J. Frish, G.W. Trucks, H.B. Schlegel, G.E. Scuseria, M.A. Robb, J.R. Cheeseman, G. Scalmani, V. Barone, B. Mennucci, G.A. Peterson, H. Nakatsuji, M. Caricato, X. Li, H.P. Hratchian, A.F. Izmaylov, J. Bloino, G. Zheng, J.L. Sonnenberg, M. Hada, M. Ehara, K. Toyota, R. Fukuda, J. Hasegawa, M. Ishida, T. Nakajima, Y. Honda, O. Kitao, H. Nakai, T. Vreven, J.A. Montgomery, Jr., J.E. Peralta, F. Ogliaro, M. Bearpark, J.J. Heyd, E. Brothers, K.N. Kudin, V.N. Staroverov, T. Keith, R. Kobayashi, J. Normand, K. Raghavachari, A. Rendell, J.C. Burant, S.S. Iyengar, J. Tomasi, M. Cossi, N. Rega, J.M. Millam, M. Klene, J.E. Knox, J.B. Cross, V. Bakken, C. Adamo, J. Jaramillo, R. Gomperts, R.E. Stratmann, O. Yazyev, A.J. Austin, R. Cammi, C. Pomelli, J.W. Ochterski, R.L. Martin, K. Morokuma, V.G. Zakrzewski, G.A. Voth, P. Salvador, J.J. Dannenberg, S. Dapprich, A.D. Daniels, O. Farkas, J.B. Foresman, J.V. Ortiz, J. Cioslowski, D.J. Fox, *Gaussian 09W, Revision C.01*, Gaussian, Inc., Wallingford CT, 2013.
- [16] (a) D.E. Woon, T.H. Dunning Jr., Gaussian basis sets for use in correlated molecular calculations. III. The atoms aluminum through argon, *J. Chem. Phys.* 98 (1993) 1358.
- (b) T.H. Dunning Jr., Gaussian basis sets for use in correlated molecular calculations. I. The atoms boron through neon and hydrogen, *J. Chem. Phys.* 90 (1989) 1007–1023.
- [17] A. Bondi, van der Waals Volumes and Radii, *J. Phys. Chem.* 68 (1964) 441–451.
- [18] According to crystal structure of **2b**, interatomic distances observed between $\pi \cdots \pi$ were 343 and 346 pm and distance between $\text{CH} \cdots \pi$ was 310 pm.
- [19] (a) P. Wen, Z. Gao, R. Zhang, An Li, F. Zhang, J. Li, J. Xie, Y. Wu, K. Guo, A- π -D- π -A carbazole derivatives with remarkable solvatochromism and mechanoresponsive luminescence turn-on, *J. Mater. Chem. C*, 5 (2017) 6136–6143.
- (b) J.Q. Tong, y. J. Wang, J. Mei, J. Wang, A. J. Qin, J.Z. Sun, B.Z. Tang, A 1,3-indandione-functionalized tetraphenylethene: aggregation induced emission, solvatochromism, mechanochromism, and potential application as a multiresponsive

fluorescent probe, *Chem. Eur. J.* 20 (2014) 4661–4670.

(c) X.Y. Shen, Y. J. Wang, E. G. Zhao, W.Z. Yuan, Y. Liu, P. Lu, A.J. Qin, Y.G. Ma, J.Z. Sun, B.Z. Tang, Effects of substitution with donor–acceptor groups on the properties of tetraphenylethene trimer: aggregation-induced emission, solvatochromism, and mechanochromism, *J. Phys. Chem. C*, 117 (2013) 7334–7347.

[20](a) Environmental Effects on Fluorescence Emission, in *Molecular Fluorescence: Principles and Applications*, B. Valeur and M.N. Berberan-Santos (Eds.), Wiley-VCH Verlag & Co. KGaA, Weinheim, 2012, ch. 5, pp. 109–140.

(b) C. Reichardt, Solvatochromic dyes as solvent polarity indicators, *Chem. Rev.* 94 (1994) 2319–2358.

[21]For related reviews on mechanism for solvatochromism, see: (a) A.S. Klymchenko, Solvatochromic and fluorogenic dyes as environment-sensitive probes: design and biological applications, *Acc. Chem. Res.* 50 (2017) 366–375.

(b) A.P. Demchenko, K.–C. Tang, P.–T. Chou, Excited-state proton coupled charge transfer modulated by molecular structure and media polarization, *Chem. Soc. Rev.* 42 (2013) 1379–1408.

[22](a) S. De Sousa, L. Ducasse, B. Kauffmann, T. Toupance, C. Olivier, Functionalization of a ruthenium–diacetylide organometallic complex as a next-generation push–pull chromophore, *Chem. Eur. J.* 20 (2014) 7017–7024.

(b) J.E. Haley, D.M. Krein, J. L. Monahan, A.R. Burke, D.G. McLean, J.E. Slagle, A. Fratini, T.M. Cooper, Photophysical properties of a series of electron-donating and -withdrawing platinum acetylide two-photon chromophores, *J. Phys. Chem. A*, 115 (2011) 265–273.

(c) A.S. Batsanov, J.C. Collings, R.M. Ward, A.E. Goeta, L. Porrès, A. Beeby, J.A.K. Howard, J.W. Steed, T.B. Marder, Crystal engineering with ethynylbenzenes Part 2. Structures of 4-trimethylsilylethynyl-N,N-dimethylaniline, and 4-ethynyl-N,N-dimethylaniline with $Z' = 12$ and a single-crystal to single-crystal phase transition at 122.5 ± 2 K, *CrystEngComm.* 8 (2006) 622–628.

(d) A. Aguilar-Granda, S. Pérez-Estrada, A. E. Roa, J. Rodríguez-Hernández, S. Hernández-Ortega, M. Rodríguez, B. Rodríguez-Molina, Cryst. Synthesis of a carbazole-[π]-carbazole molecular rotor with fast solid state intramolecular dynamics and crystallization-induced emission, *Growth Des.* 16 (2016) 3435–3442.

(e) C. Quinton, V. Alain-Rizzo, C. Dumas-Verdes, G. Clavier, L. Vignau, P. Audebert, Triphenylamine/tetrazine based π -conjugated systems as molecular donors for organic solar cells, *New. J. Chem.* 39 (2015) 9700–9713.

(f) E.S.–H. Lam, D.P.–K. Tsang, W.H. Lam, A.Y.–Y. Tam, M.–Y. Chan, W.–T. Wong, V.W.–W. Yam, Luminescent platinum(ii) complexes of 1,3-bis(n-alkylbenzimidazol-2'-yl)benzene-type ligands with potential applications in efficient organic light-emitting diodes, *Chem. Eur. J.* 19 (2013) 6385–6397.

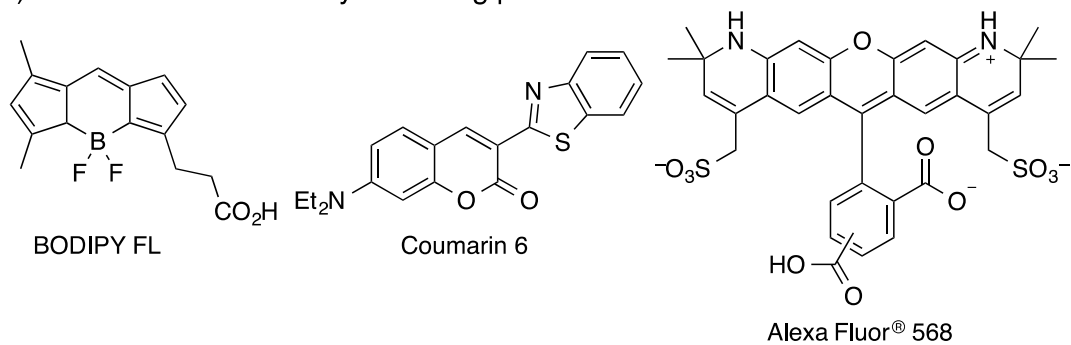
(g) Y.–G. Zhi, S.–W. Lai, Q.K.–W. Chan, Y.–C. Law, G.S.–M. Tong, C.–M. Che, Systematic studies on photoluminescence of oligo(arylene-ethynylene)s: tunability of excited states and derivatization as luminescent labeling probes for proteins, *Eur. J. Org. Chem.* (2006) 3125–3139.

(h) C.S. Kim, Y.J. Cho, H.J. Kwon, B.O. Kim, S. M. Kim, *PCT Int. Appl.*, 2011111930.

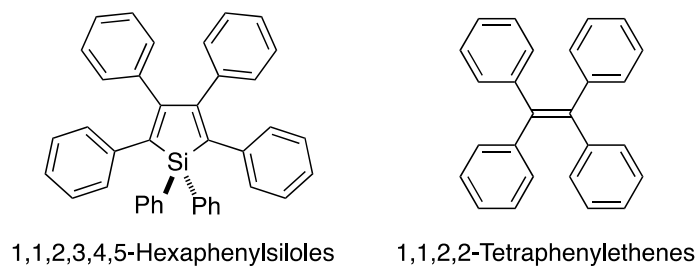
[23](a) G.M. Sheldrick, SHELXS-2014, Program for Crystal Structure Solution, University of Göttingen, 2014.

(b) G.M. Sheldrick, A short history of SHELX, *Acta Crystallogr., Sect. A: Fundam. Crystallogr.* 64 (2008) 112–122.

(A) Common fluorescent dye showing photoluminescence in dilute solution



(B) AIEE-/CIEE-active molecule showing photoluminescence in solid state



(C) Fluorophore showing photoluminescence both in solution and in solid state

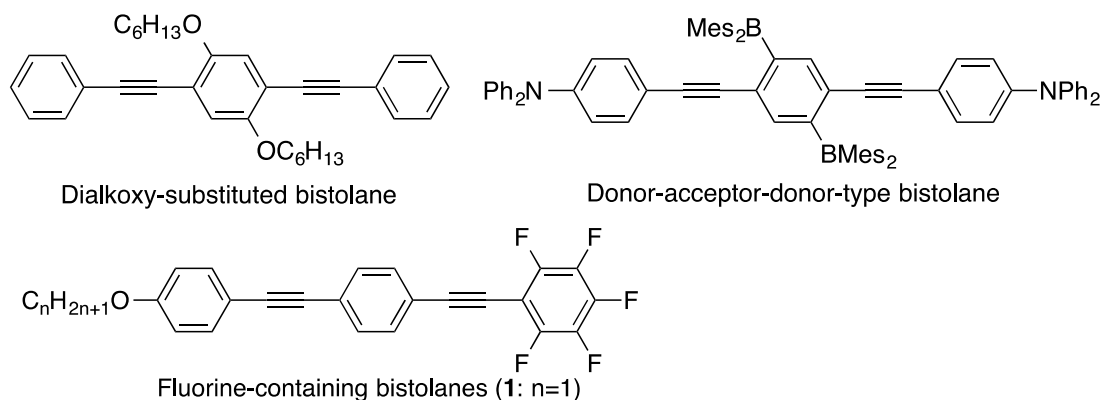


Fig. 1 Classification of fluorescent materials according to the state of molecules

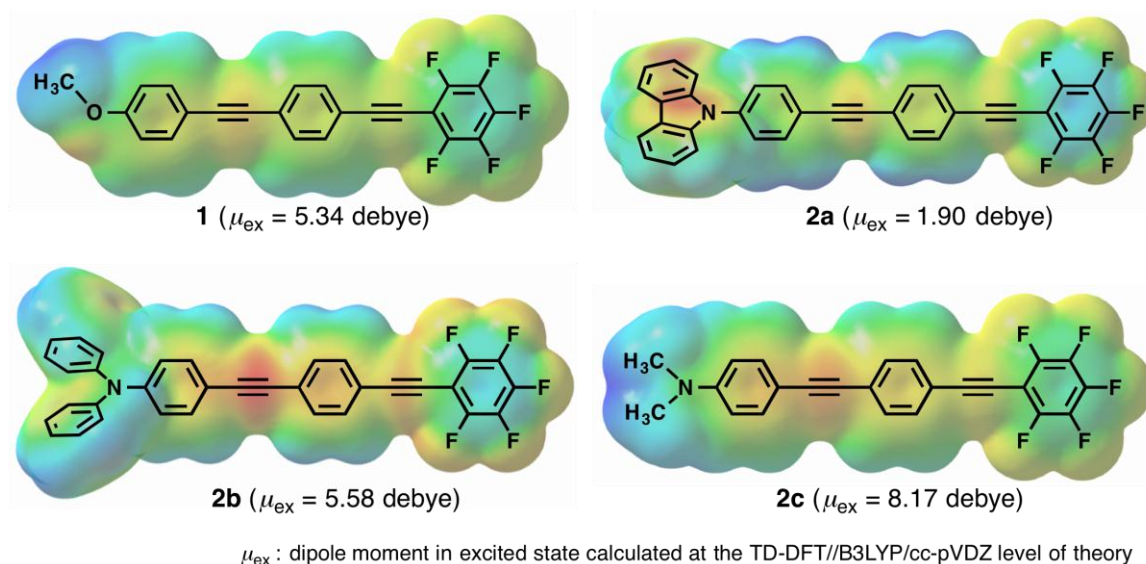


Fig. 2 Electrostatic potential distribution of **1** and **2**. Computations were performed for optimized geometries at the DFT/B3LYP/cc-pVDZ levels of theory. The density isosurface value is 0.005, and negatively and positively charged regions are indicated by red and blue, respectively. μ_{ex} indicates dipole moment in the excited state at the Franck-Condon geometry (B3LYP/aug-cc-pVDZ levels of theory).

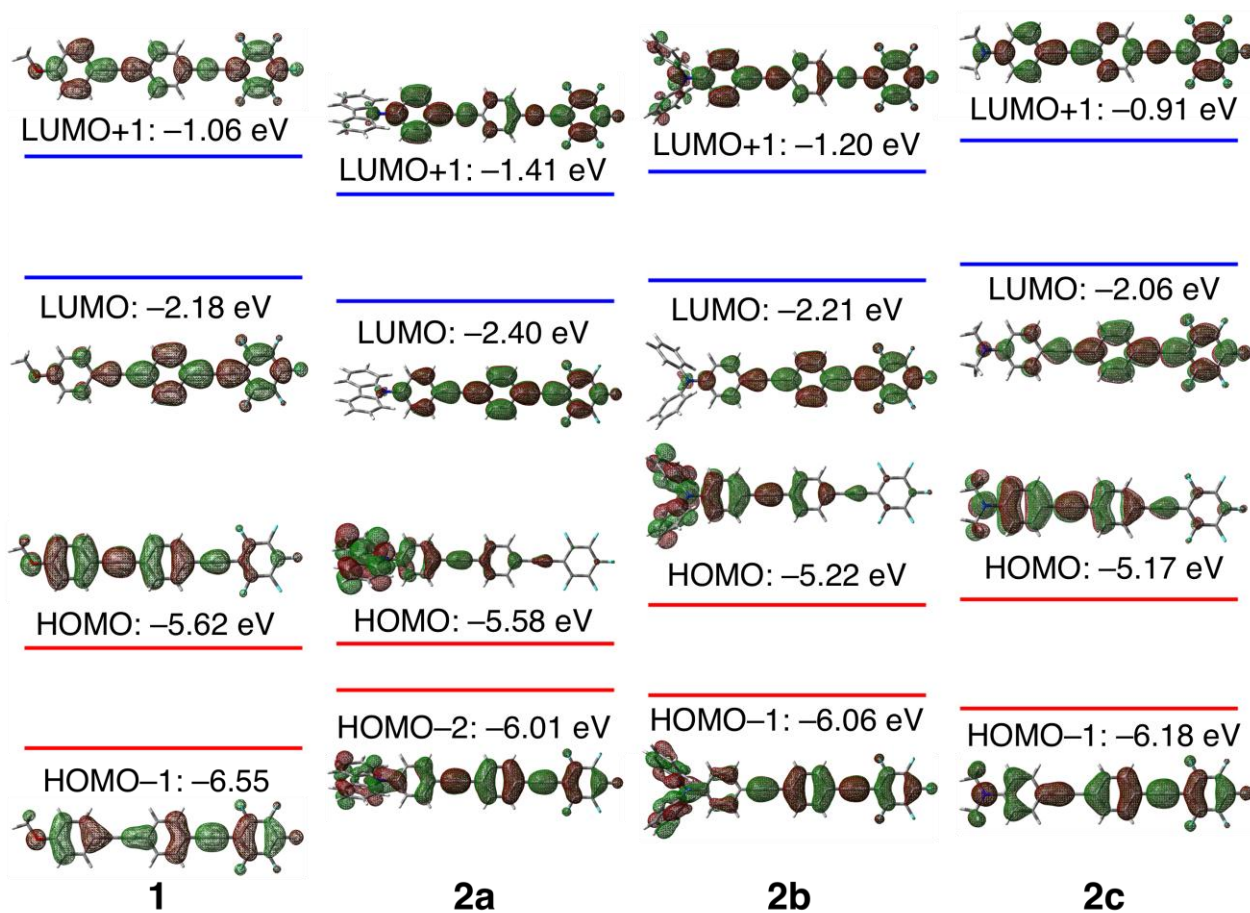


Fig. 3 Molecular orbitals (HOMO-1, HOMO, LUMO, and LUMO+1) for **1** and **2** computed at the

TD-DFT/B3LYP/aug-cc-pVDZ levels of theory, and the corresponding orbital energies in the ground state.

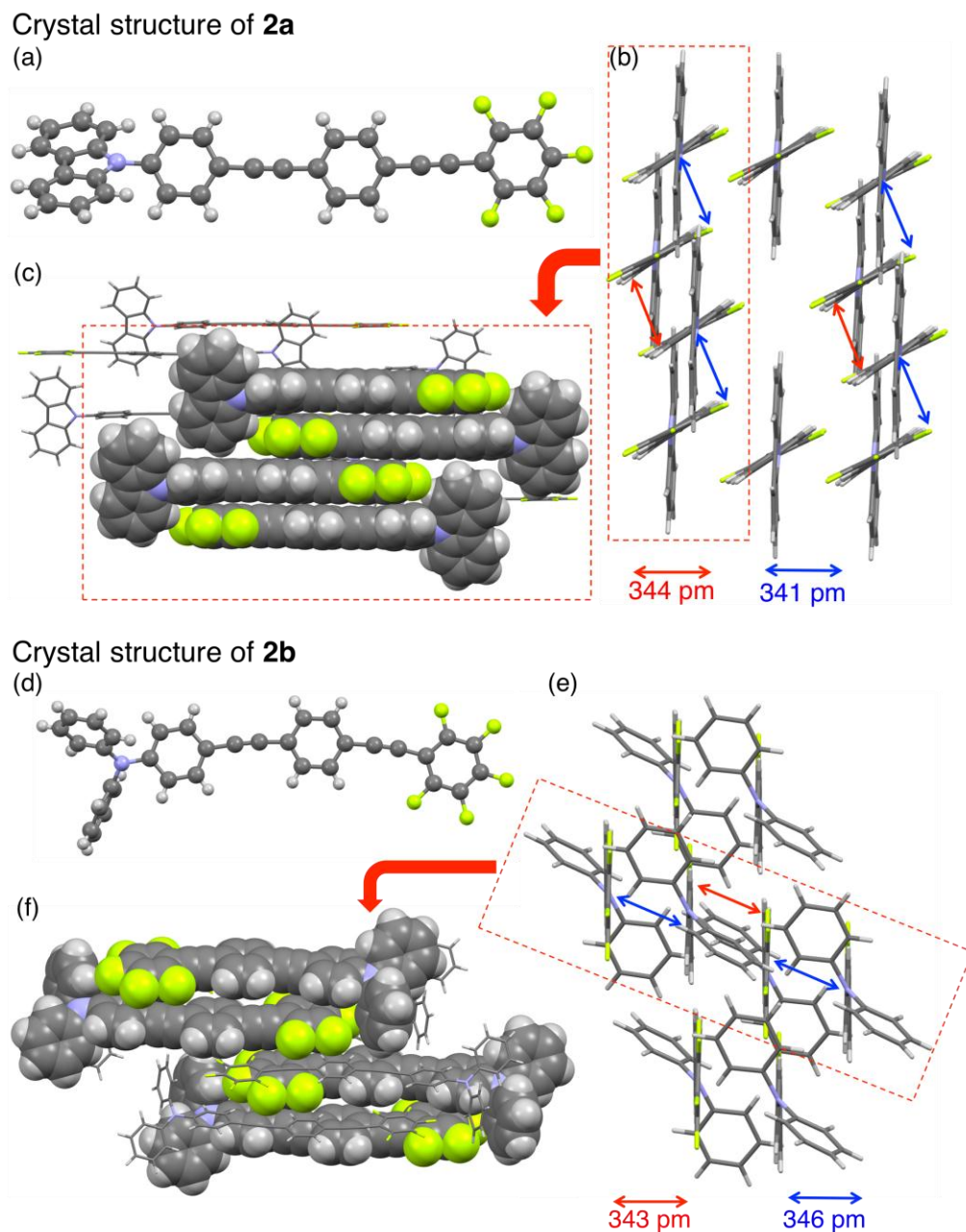


Fig. 4 Crystal structures of **2a** and **2b**. (a), (d) Molecular structures in the crystal. (b) Packing structure of **2a** and (c) space-filling model viewing at the red-square region. (e) Packing structure of **2b** and (f) space-filling model viewing at the red-square region. Color legend: C: grey, H: light-grey, N: blue, and F: light-green.

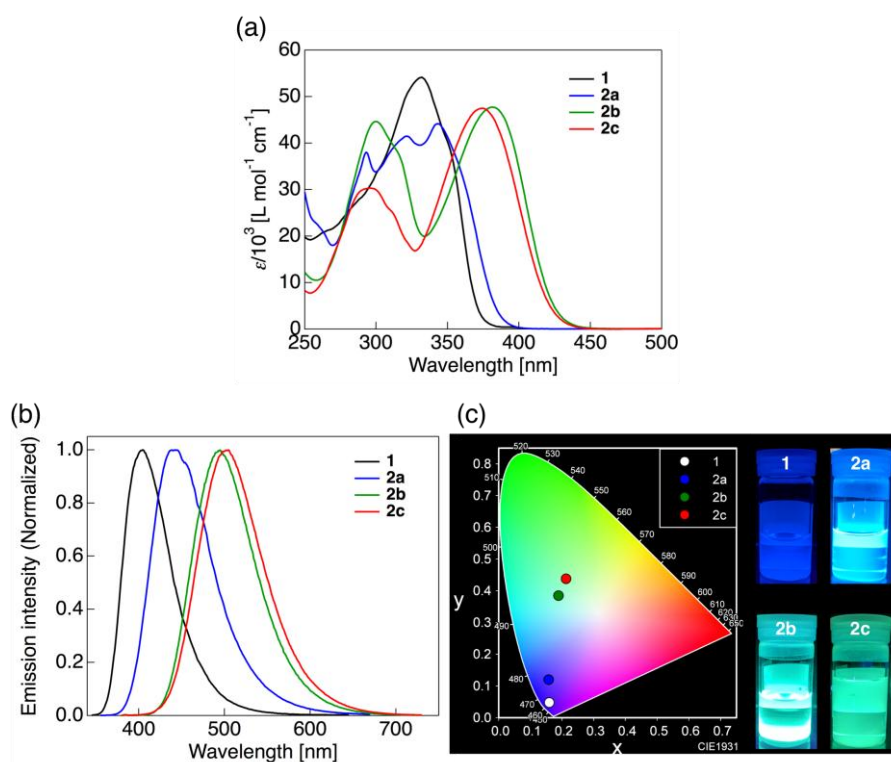


Fig. 5 (a) Absorption spectra of **1** and **2a–c** in CH_2Cl_2 (10^{-5} mol L^{-1}). (b) Corrected photoluminescence spectra of **1** ($\lambda_{\text{ex}} = 330$ nm), **2a** ($\lambda_{\text{ex}} = 342$ nm), **2b** (372 nm) and **2c** ($\lambda_{\text{ex}} = 372$ nm) in CH_2Cl_2 (10^{-6} mol L^{-1} concentration). (c) Color diagram of the photoluminescence observed for **1** and **2a–c**, and photographs under UV irradiation ($\lambda_{\text{ex}} = 365$ nm).

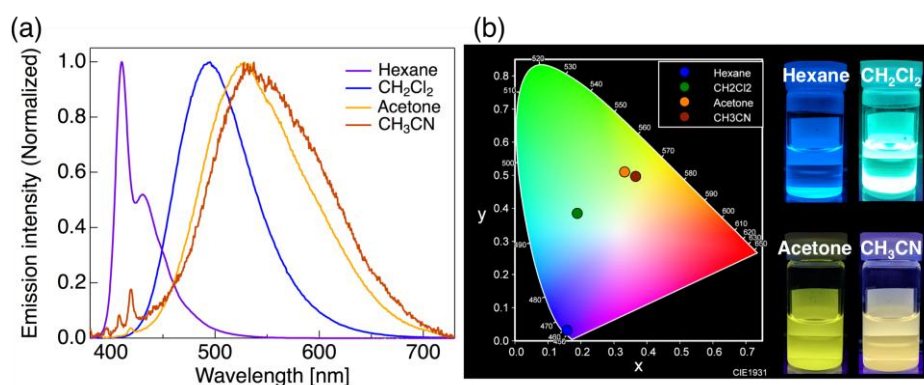


Fig. 6 (a) Photoluminescence behavior of **2b** measured in various solvents (10^{-6} mol L^{-1} concentration, $\lambda_{\text{ex}} = 372$ nm). (b) Color diagram of photoluminescence observed for **2b** depending on solvent polarity (dielectric constant (ϵ) for hexane: 1.88, CH_2Cl_2 : 8.93, acetone: 20.6, and for acetonitrile: 35.9), and photographs under UV irradiation ($\lambda_{\text{ex}} = 365$ nm).

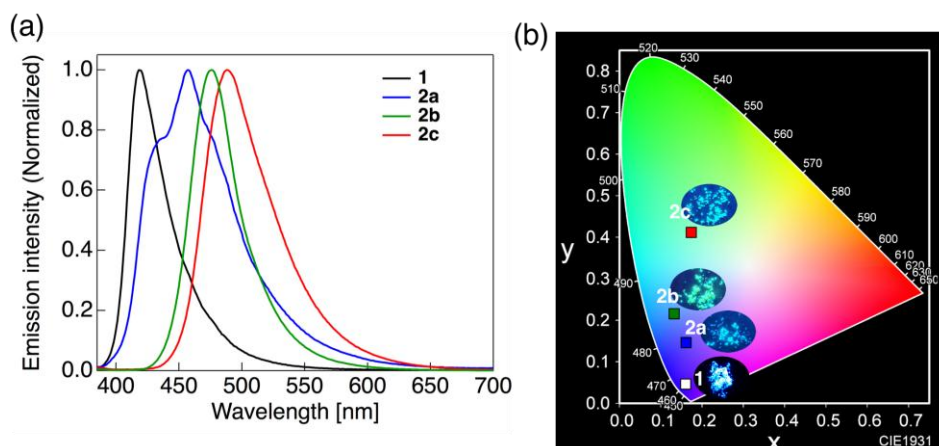


Fig. 7 (a) Corrected photoluminescence spectra of **1** ($\lambda_{\text{ex}} = 365$ nm), **2a** ($\lambda_{\text{ex}} = 371$ nm), **2b** ($\lambda_{\text{ex}} = 365$ nm), and **2c** ($\lambda_{\text{ex}} = 371$ nm) in the solid state. (b) Color diagram of the emission of **1** and **2a-c**. Inset: photographs of the compounds in the solid state under UV irradiation ($\lambda_{\text{ex}} = 365$ nm).

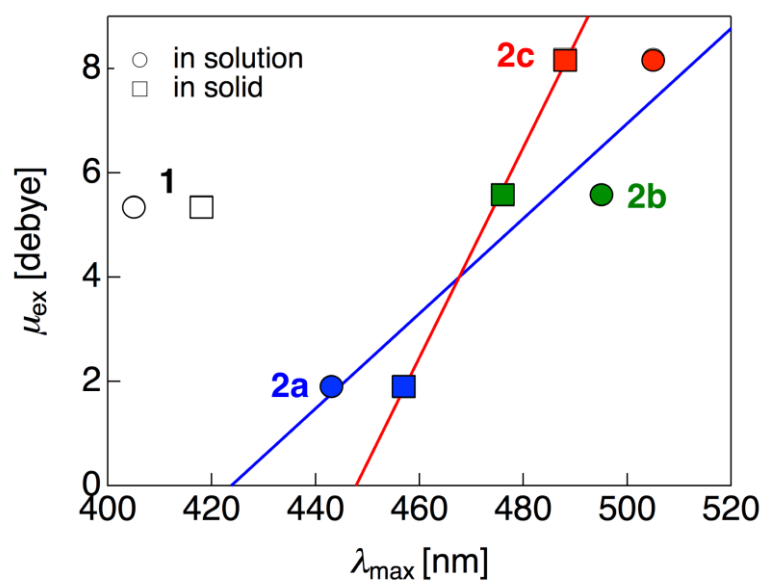
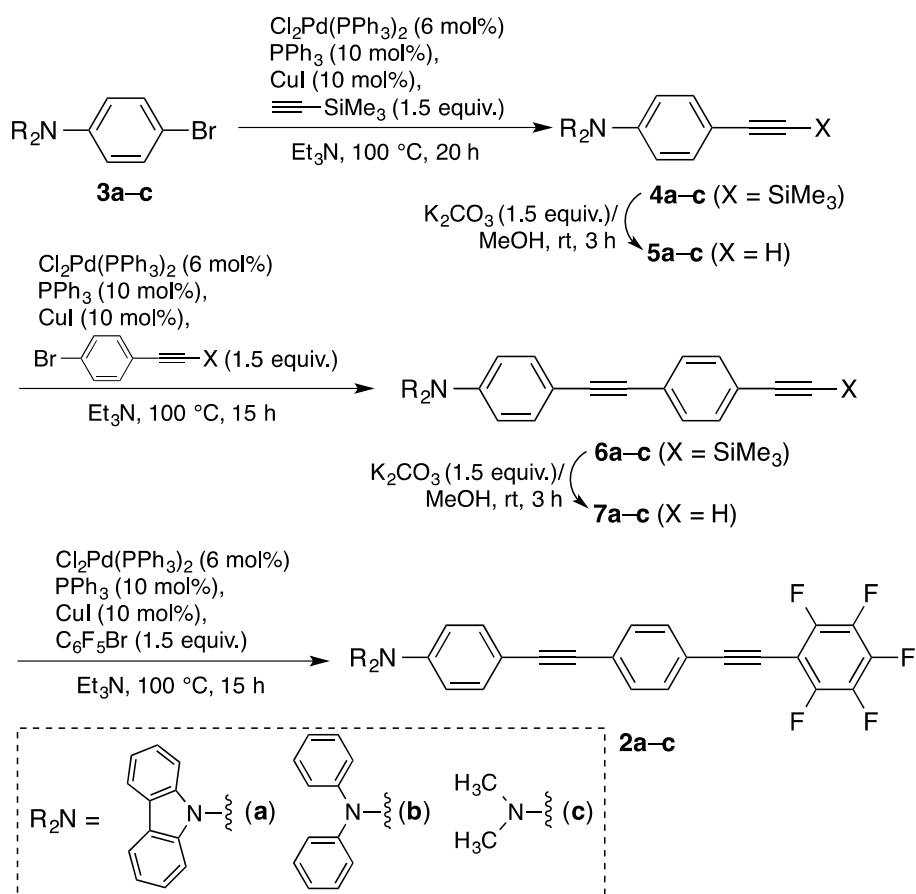


Fig. 8 Relationship between molecular dipole moment in an excited state (μ_{ex}) and photoluminescence maximum wavelength (λ_{max}). Plots, \circ and \square , indicate measurements in solution and in the solid state, respectively, for **1** (white), **2a** (blue), **2b** (green) and **2c** (red). Blue line shows a linear fitting function obtained by a least-squares regression among **2a-c** in solution, and the red line also the linear fitting estimated from **2a-c** in the solid state.



Scheme 1. Synthetic pathway for the novel fluorinated bistolanes with *N*-type electron-donating substituent

Table 1. Theoretical parameters for **1** and **2** computed using the DFT or TD-DFT method in the gas phase^a

Compd.	HOMO-1 / HOMO [eV] ^a	LUMO / LUMO+1 [eV] ^a	Calculated electronic transitions ^b		
			Wavelength [nm]	Composition (molecular contribution, %)	<i>f</i> ^c
1	-6.55 / -5.62	-2.18 / -1.06	398	HOMO → LUMO (99%)	1.67
			319	HOMO-1 → LUMO (72%) HOMO → LUMO+1 (26%)	0.40
2a	-6.01 ^d / -5.58	-2.40 / -1.41	441	HOMO → LUMO (99%)	0.76
			365	HOMO-2 → LUMO (98%)	1.54
2b	-6.06 / -5.22	-2.21 / -1.20	464	HOMO → LUMO (98%)	1.28
			355	HOMO-1 → LUMO (72%) HOMO → LUMO+1 (26%)	1.11
2c	-6.18 / -5.17	-2.06 / -0.91	439	HOMO → LUMO (99%)	1.38
			330	HOMO-1 → LUMO (72%) HOMO → LUMO+1 (26%)	0.91

^a Theoretical calculations were performed by the DFT method using Gaussian09 program package. The geometry optimizations and frequency calculations were performed with a standard basis set at the B3LYP/cc-pVDZ level of theory. ^b Calculated by the TD-DFT method at the B3LYP/aug-cc-pVDZ levels of theory for optimized geometry. ^c Oscillator strength. ^d Shown orbital energy at HOMO-2 involves electronic transition.

Table 2. Photophysical data for **1** and **2a–c** in CH₂Cl₂ solution

Compound	Absorption in solution ^a	Emission in solution ^b
	λ_{abs} [nm] ($\epsilon/10^3$ [L mol ⁻¹ cm ⁻¹])	$\lambda_{\text{em}} / \Phi_{\text{em}}$
1	332 (54.2), 350 (shoulder, 40.3)	405 / 0.79
2a	293 (38.1), 321 (41.5), 343 (44.2)	443 / 0.87
2b	300 (44.7), 313 (shoulder, 39.0), 381 (47.7)	495 / 0.89
2c	296 (30.3), 311 (shoulder, 25.2), 374 (47.5)	505 / 0.84

^a Measured in 10⁻⁵ mol L⁻¹ CH₂Cl₂ solution. ^b Measured in 10⁻⁶ mol L⁻¹ CH₂Cl₂ solution.

Table 3. Photophysical data in the solid state

Compound	Emission in solid	
	λ_{em}	Φ_{em}
1	418	0.66
2a	436, 457	0.46
2b	476	0.43
2c	488	0.11